DOI: https://doi.org/10.47275/2332-4864-117
Volume 6 Issue 2
Research Article

Scholit Publishers

Journal of Clinical & Anatomic Pathology

Adoption of Optical Genome Mapping in Clinical Cancer Cytogenetic Laboratory: A Stepwise Approach

Victoria Stinnett[1,2,3], Liqun Jiang[2,3], Lisa Haley[2,3], Candice Ament[1,2,3], Melanie Hardy[1,2,3], Laura Morsberger[1,2,3], Jennifer Ghabrial[1,2,3], Raluca Yonescu[1,2,3], Emily Adams[2,3], Patty Long[1,2,3], James R Eshleman[2,3], Christopher D Gocke[2,3] and Ying S Zou[1,2,3]*

[1]Clinical Cytogenetics Laboratory, Johns Hopkins University School of Medicine, Baltimore, USA
[2]Johns Hopkins Genomics, Johns Hopkins University School of Medicine, Baltimore, USA
[3]Department of Pathology, Johns Hopkins University School of Medicine, Baltimore, USA

Abstract

Detection of Chromosomal Abnormalities (CA) is important for cancer patients. Compared to common cancer cytogenetics methods including karyotype, fluorescent in situ hybridization (FISH), and chromosomal microarray (CMA), optical genome mapping (OGM) is an innovative method to detect CA. The objective of this pilot study was to determine a stepwise approach to adopt OGM in the clinical setting. A blinded study was used to compare OGM, karyotype, FISH, and CMA on five cancer cases (four leukemia/lymphoma and one solid tumor). Next-generation sequencing and a gene fusion assay were also used for confirmation. We used a stepwise approach to analyze OGM calls. Three-quarters of 406 OGM calls in this study were filtered out according to genomic sizes, cancer genes, and knowledge-based cancer databases. The remaining 89 calls were analyzed independently/blindly to determine their reportability/ pathogenicity. OGM revealed all chromosome abnormalities previously identified by karyotype and FISH (a total of 98 loci) and achieved a sensitivity of 100%. Compared to CMA, the sensitivity of OGM was 88% (including copy-number neutral loss of heterozygosity (CN-LOH)) and 96% (excluding CN-LOH). While, OGM cannot detect CN-LOH, while it revealed 71 additional calls, 52% of breakpoints involved genes and 7.7% of breakpoints involved known cancer genes. Although these additional/unrecognized calls may play roles in cancer development and formation, they are currently variants of unknown clinical significance. OGM effectively characterized a complex rearrangement and a chromothripsis-like event. OGM is a reliable method for detecting both copy number variants and structural variants in cancer genomes using a stepwise approach and can be adopted smoothly into the clinical setting as a promising alternative to routine cytogenetic techniques of karyotype/FISH/CMA assays.

Keywords: Chromosomal abnormalities; Structural chromosome abnormalities; Copy number variants; Optical genome mapping; Cancer cytogenetics

Introduction

Chromosomal abnormalities, including copy number variants (CNVs) and structural variants (SVs), are important in cancer patients, as they can inform targeted therapeutic decisions, prognostic risk stratification, and relapse prediction [1,2]. Therefore, the detection of CNVs and SVs in cancer patients is of great diagnostic value [1-3]. Routine cancer cytogenetic techniques used for detecting chromosome abnormalities include conventional chromosome analysis/karyotype, fluorescent in situ hybridization (FISH), and whole-genome chromosomal microarray assays (CMA). A karyotype can detect genome-wide CNVs and SVs at the limit of resolution of 5 - 10 Mb and is commonly time-consuming. FISH is locus-specific depending on specific probes for evaluating limited CNVs and SVs in the genome. Large FISH panels containing numerous probes can detect more loci but become more expensive. CMA can detect genome-wide CNVs at a resolution that is ~ 100x more sensitive than karyotype. However, CMA cannot detect any balanced SVs such as inversions, reciprocal translocations, and insertions, or any additional balanced complex rearrangements, which may act as oncogenic driver mutations in cancers [1,2].

Optical genome mapping (OGM) technology is an innovative single-molecule method that can detect both CNVs and balanced/unbalanced SVs [4-10]. It is a high-throughput and whole-genome analysis system that generates ordered restriction maps from high molecular weight genomic DNA molecules, ranging in size from 300 kilobases (Kb) to a few megabases (Mb) [4,7 and 9-13]. Computational approaches are used for the construction of genome-wide physical restriction maps of patient samples [4,14-18]. It provides insights into long-range genome structure and genome variation and effectively detects genome-wide CNVs and SV [4,7-13]. It has been used as a tool/method to guide and/or validate

***Correspondence to:** Ying S Zou, Director of Cancer Genetics Lab, Co-director of Cytogenetics and Genomics Lab, Associate Director of Molecular Diagnostic Lab, JH Genomics, Associate Professor of Genetic Medicine and Pathology, Johns Hopkins University School of Medicine, 1812 Ashland Ave., Suite 221 Baltimore, MD 21205, USA; E-mail: yzou19@jhmi.edu

Citation: Stinnett V, Jiang L, Haley L, et al. (2021) Adoption of Optical Genome Mapping in Clinical Cancer Cytogenetic Laboratory: A Stepwise Approach. J Clin Anat Pathol, 6(2): 117. DOI: https://doi.org/10.47275/2332-4864-117

Received: April 13, 2021; **Accepted:** May 21, 2021; **Published:** May 24, 2021

DNA sequencing-based genome assemblies [7-13], to identify structural polymorphisms/ variations in normal human genomes [5,6 and 19], to study functional methylome [20] and viral insertions [21], and to detect abnormal repeats in human diseases [22-25], oncogene amplification [26], germline CNVs and SVs in known disease-risk and disease regions [27-29], and CNVs and SVs in cancer genomes [30-36].

Because OGM detects both CNVs and SVs in a single workflow without an amplification step, it has recently demonstrated potential clinical utility in clinical cancer cytogenetics laboratories [4,30-34,36 and 37]. The objective of this pilot study was to determine a stepwise approach to adopt OGM in the clinical setting. A set of five clinical cancer cases including four leukemia/lymphoma samples and one fresh solid tumor specimen were analyzed by OGM and simultaneously tested with karyotype, leukemias/ lymphomas FISH panels, a targeted next-generation sequencing (NGS) DNA mutation assay, and a gene fusion assay. We used a stepwise approach to analyze OGM calls independently and blindly, to determine the feasibility of adopting OGM as a routine test into a clinical cancer cytogenetic laboratory.

Materials and Methods

Clinical specimens

This study included five consecutive clinical cancer specimens from 01/01/2020 to 05/01/2020 that were referred to cytogenetic studies and had enough material for simultaneous optical genome mapping. They consist of four leukemia/lymphoma specimens (one EDTA peripheral blood and three EDTA bone marrow samples) and one solid tumor specimen (fresh kidney tumor tissue).

Optical genome mapping (OGM)

Ultra-high molecular weight DNA was extracted from peripheral blood, bone marrow aspirates, or fresh solid tumor tissue specimen, according to the manufacturer's protocols (Bionano Genomics Inc., San Diego, CA). DNA was quantified with Qubit dsDNA assay kits (Thermo Fisher Scientific, Waltham, MA). DNA labeling was performed according to the manufacturer's protocols (Bionano Genomics Inc., San Diego, CA). Briefly, standard direct label enzyme 1 reactions were performed using 750 ng of purified high molecular weight DNA per specimen with the counterstained DNA backbone. Labeled DNAs were loaded on Saphyr chips, and were imaged sequentially across nanochannels on a Saphyr instrument (Bionano Genomics Inc., San Diego, CA).

Genome analysis was performed using software solutions provided by Bionano Genomics (Bionano Access and Bionano Solve, last accessed on 10/5/2020, Bionano Genomics Inc., San Diego, CA) to identify potentially somatic variant calls. Rare variant pipeline analysis was performed to sensitively capture somatic SVs occurring at low allelic fractions and copy number variant pipeline analysis for whole arm numerical abnormalities, terminal deletions, or unbalanced translocations with centromeric breakpoints according to manufacturer's protocols (Bionano Genomics Inc., San Diego, CA).

A blinded study was performed to analyze OGM calls. We used a stepwise approach to analyze all OGM calls. First, we filtered all calls according to genomic size. The size threshold is based on genomic size used by our current SNP microarray for cancer specimens, which is also close to the CAP recommended criteria when submitting oncology microarray proficiency testing. Second, we filtered all calls according to well-defined cancer genes and cancer-related genes (Supplemental Table S2, gene lists from CGC (https://www.cancergenomics.org/databases_ and_ gene_ lists.php), and COSMIC's cancer gene census (https://cancer.sanger.ac.uk/census)). Third, we compared these abnormalities according to knowledge-based cancer databases (The Atlas of Genetics and Cytogenetics in Oncology and Haematology (http://atlasgeneticsoncology.org/), the Cancer Genome Atlas Copy Number Portal (http://portals.broadinstitute.org/tcga/gistic/ browseGisticAnalyses), the Mitelman database (https://mitelmandatabase.isb-cgc.org/), COSMIC (https://cancer.sanger. ac.uk/cosmic), the ICGC data portal (https://dcc.icgc. org/), the cBioPortal (http://www.cbioportal.org/), the National Cancer Institute Genomic Data Commons (https://portal.gdc.cancer.gov/), My Cancer Genome (https://www.mycancergenome.org/), and Online Mendelian Inheritance in Man (https://www.ncbi.nlm.nih.gov/omim/)). All filtered calls that met these criteria were analyzed independently by cytogenetic technologists proficient in analyzing whole-genome CMA data. Calls were presumed to be germline if they were present at 100% frequency and have been previously identified in constitutional microarrays as a benign structural variation (polymorphism) in the normal human genome (such as Database of Genomic Variants (http://dgv.tcag.ca/ dgv/app/home)). We also analyzed genes at breakpoints of calls, within 10 kb at the SV breakpoint start and end positions of insertions/deletions/ duplications, and within 50 kb for inversions/ translocations. A final clinical report including all reportable abnormalities was generated, and all calls identified by optical mapping were annotated into a JHU-cancer cytogenetic database and BED file to use in the UCSC genome browser.

Whole-genome SNP microarray

SNP microarray was performed with DNA extracted from bone marrow and peripheral blood specimens (QIAamp® DNA Midi Spin Kit and Qiacube®, QIAGEN, Hilden, Germany) and solid tumor specimen (Gentra Puregene® Tissue Kit, QIAGEN, Hilden, Germany) specimens by conventional methods (Qiagen, Hilden, Germany). DNA concentration was assessed using the Qubit fluorometer and/or NanoDrop 2000 spectrophotometer (Thermo Fisher Scientific, Waltham, MA). The high-resolution microarray platform utilized was the Illumina Infinium CytoSNP-850K v1.2 BeadChip containing over 850,000 markers (mean spacing 3.5 kb) (Illumina, Inc. USA). BeadChips were processed per manufacturer's guidelines and imaged with the Illumina iScan system. Data were analyzed with the CNV Partition 2.4.4.0 algorithm with GenomeStudio (v2010.3, Illumina) and KaryoStudio (v1.4.3.0, Illumina). B - allele frequency and LogR signal intensities were used to examine and identify potentially pathogenic regions of genomic imbalance. All analysis was performed using human reference genome assembly hg19 (GRCh37).

Targeted next-generation sequencing (NGS) assay

DNA was extracted from blood and bone marrow specimens by conventional methods (Qiacube, Qiagen, Hilden, Germany). DNA was extracted from solid tumor tissue specimens with the Siemens TPS automated method (Siemens Healthineers, Malvern, PA). DNA concentration

was assessed using the Qubit fluorometer using either DNA-HS or DNA-BR reagents according to vendor specification (Thermo Fisher Scientific, Waltham, MA). Library preparation was performed using Kapa Roche HyperPrep reagents, hybrid capture performed using Integrated DNA Technologies probes, and products sequenced using NovaSeq (Illumina paired-end technology). The targeted NGS assay used 40,670 Integrated DNA Technologies probes and for a list of covered cancer genes in the targeted NGS assay, see https://pathology.jhu.edu/jhml-services/assets/test-directory/HemePanel_GeneList_ v5.0.pdf. Analysis was performed using human reference sequence genome assembly hg19 (NCBI build GRCh37/hg19). An in-house variant and CNV caller software (MDL VC 10) and CNVkit software version 0.9.5 (https://cnvkit.readthedocs.io/en/stable/, last accessed on February 1st, 2021) were used to generate gene variants/mutations and genome-wide copy number variants from the targeted NGS data.

Targeted gene fusion panel

Bone marrow aspirate or peripheral blood specimens were drawn into lavender top tubes containing EDTA were processed using the QIAamp RNA Blood Mini Kit, Cat#52304, (Qiagen, Beverly, MA), according to vendor specifications, with 2 to 12 mL of each specimen. For solid tissue, after macro-dissection to enrich for tumor, RNA was isolated utilizing the Siemens Tissue preparation automated bead-based method with Versant TPS reagents according to vendor protocol (Siemens Healthineers, Malvern, PA). RNA concentration was assessed using the QUBIT fluorometer with RNA-HS or RNA-BR reagents according to vendor directions (Thermo Fisher Scientific, Waltham, MA).

Probe design and construction were performed in collaboration with NanoString Technologies. nCounter Element reagents were purchased from NanoString, and probes were synthesized by IDT (Coralville, IA). Sample processing was performed using the nCounter Prep Station (NanoString Technologies), and RNA counting was performed using the nCounter digital analyzer (NanoString Technologies) following the manufacturer's protocol. Raw counts directly from the nCounter digital analyzer were subjected to normalization using the internal positive spike-in controls by nSolver analysis software version 4.0 (NanoString Technologies), followed by probe-specific background correction. A fusion transcript was considered as expressed if the count number was beyond the normal range, defined as the upper quantile (Q3) plus 3 times the interquartile range in the boxplot. The full list of covered fusion and gene expression imbalance targets is on the website (https://pathology.jhu.edu/Molecular Diagnostics/tests.cfm).

Karyotype and Fluorescence *in situ* hybridization (FISH)

Conventional G-banded chromosome studies were performed using standard techniques. A minimum of 20 metaphase cells were analyzed from unstimulated bone marrow aspirate, peripheral blood, or solid tumor cultures. The abnormal karyotypes were described using the International System for Human Cytogenetic Nomenclature (ISCN 2016). FISH was performed on interphase nuclei using disease-specific panels of probes according to the manufacturer's protocol (Abbott Molecular Inc., Des Plaines, IL). The CLL FISH panel includes 6CEN (*D6Z1*), 6q23.3 (*MYB*), 11CEN (*D11Z1*), 11q22.3 (*ATM*), 12CEN (*D12Z3*), 12q15 (*MDM2*), 13q14.3 (*D13S319*), 13q34 (*LAMP1*), 11q13 (*CCND1*), and 14q32 (*IGH*) probes (Abbott Molecular Inc., Des Plaines, IL). The B-ALL FISH panel includes 1q23 (*PBX1*), 19p13.3 (*TCF3*), 4CEN (*D4Z1*), 10CEN (*D10Z1*), 17CEN (*D17Z1*), 8q24 (*5'MYC,3'MYC*), 9p21 (*CDKN2A*), 9CEN (*D9Z1*), 9q34 (*ABL1*), 22q11.2 (*BCR*), 11q23 (5'MLL[*KMT2A*], 3'MLL[*KMT2A*]), 12p13 (*ETV6*), 21q22 (*RUNX1*), 14q32 (*3'IGH,5'IGH*), 17p13 (*TP53*), 17CEN (*D17Z1*), Xp22.33/Yp11.32 (*3'CRLF2, 5'CRLF2*), and Xp22.33/Yp11.32 (*3'P2RY8, 5'P2RY8*) (Abbott Molecular Inc., Des Plaines, IL). The AML/MDS FISH panel includes 3q21 (*RPN1*), 3q25.32 (*MLF1*), 3q26.2 (*MECOM*), 4q21 (*AFF1*), 5p15.2 (*D5S630*), 5q31 (*EGR1*), 5q35.1 (*NPM1*), 6p23 (*DEK*), 6q27 (*MLLT4*), 7CEN (*D7Z1*), 7q31 (*D7S486*), 8p11.2 (*KAT6A*), 8CEN (*D8Z2*), 8q22 (*RUNX1T1*), 8q24.1 (*MYC*), 9p22 (*MLLT3*), 9q34 (*ABL1*), 9q34 (*NUP214*), 10p12 (*MLLT10*), 11p15.4 (*3'NUP98, 5'NUP98*), 11q23 (*5'MLL [KMT2A],3'MLL[KMT2A]*), 13q14.3 (*D13S319*), 13q34 (*LAMP1*), 15q24.1 (*PML*), 16p13.3 (*CREBBP*), 16p13 (*MYH11*), 16q22 (*CBFB*), 17p13 (*TP53*), 17q21 (*RARA*), 17CEN (*D17Z1*), 19p13.1 (*ELL*), 19p13.3 (*MLLT1*), 20q12 (*D20S108*), 20q13.2 (*ZNF217*), 21q22 (*RUNX1*), and 22q11.2 (*BCR*) (Abbott Molecular Inc., Des Plaines, IL). The X/Y FISH included XCEN (*DXZ1*) and YCEN (*DYZ1*) probes (Abbott Molecular Inc., Des Plaines, IL). A total of 200 nuclei per probe were evaluated with fluorescence microscopy by two technologists scoring blinded from each other using a Zeiss Axioscope system. The analysis was performed using Cytovision software (Leica Inc., Buffalo Grove, IL). The specimen was considered abnormal if the results exceeded the laboratory-established cut-off for each probe set.

Results

CNVs and SVs by routine cytogenetic tests

Karyotype, FISH, and CMA of five specimens detected two abnormal karyotypes, seven positive FISH loci among a total of 98 loci tested, and twenty-five calls by CMA (Table 1). Combination of all three techniques showed a total of twenty-three CNVs, five SVs, and two regions of copy-number neutral loss of heterozygosity (CN-LOH) (Table 1 and Supplemental Table S1).

CNVs and SVs by OGM

Specimens tested in this study had an ultra-high molecular weight DNA concentration ranging from 42 to 131 ng/μL. OGM collected data (~1300 Gb per specimen), which achieved an effective genome coverage of over 400x. Molecule N50 (for molecules >150 kb) values were greater than 250kb. OGM generated ~2,099 calls per specimen (Table 1). Approximately 81 calls per specimen in this study were obtained after analyzing using Bionano software (Bionano Genomics Inc., San Diego, CA).

We obtained ~ 18 calls per specimen after applying the above three filters (Table 1), which eliminated ~ 75% of OGM calls and reduced analysis time. We analyzed the calls independently, manually, and achieved consistent results among analyzers. OGM revealed two unbalanced translocations and two deletions that were detected by karyotype (Supplemental Table S1) and achieved a sensitivity of 100%. It also detected three gene fusions (*NUP98/NSD1*, *BCR/ABL1*, and *MLLT3/KMT2A*), a complex 11;14 rearrangement, and two deletions that were detected by FISH

Table 1: Overview of clinical, cytogenetic and OGM data in this study.

Sample	**1**	**2**	**3**	**4**	**5**	**Total number**
Tissue source	Bone marrow	Bone marrow	Peripheral blood	Bone marrow	Kidney tumor fresh tissue	3
Tumor type	AML	CLL	B-ALL	AML	Wilms' tumor, blastema-predominant	4
Karyotype	46,XY[20]	46,XY[20]	46,XY[20]	46,XX,der(9)t(9;11)(p21;q23),der(11) del(11)(p11.2p13) t(9;11) (p21;q23)[10]//46,XY[10]	46,XY,del(3)(p12 p12),add(14)(q23) [20]	2 abnormal karyotypes
FISH	*NUP98/NSD1* fusion by AML/MDS panel	Normal AML/MDS and CLL panels	*BCR/ABL1* fusion and loss of *CDKN2A* and *ETV6* by B-ALL panel	*MLLT3/MLL* fusion by AML/MDS FISH panel and XX/XY cells by X/Y FISH	der(14)t(11;14) by a metaphase FISH	7 abnormal FISH
SNP microarray (CMA)	4	7	6	4	4	25
All OGM calls	2,207	2,090	2,034	2,169	1,997	10,497
OGM calls after Bionano pipelines	89	54	121	89	53	406
OGM calls >250 kb	16	11	12	8	6	53
OGM calls < 250kb with cancer genes	2	6	5	2	5	20
Additional OGM calls with SV	5	3	3	4	1	16
Total OGM calls identified for review	23	20	20	14	12	89

assays among a total of 98 probe loci tested in this study (Supplemental Table S1) and achieved a sensitivity and specificity of 100%.

Compared to CMA, OGM revealed 22 of 23 CNVs (96%) and did not detect a low-level gain of the whole short arm of chromosome 6 (case 2 in Table 2). OGM did not detect two regions of CN-LOH as expected (Table 2). Therefore, the sensitivity of OGM was 96% (excluding CN-LOH calls by CMA) and 88% (including CN-LOH calls by CMA) compared to CMA. OGM revealed 71 additional calls including 51 CNVs and 20 SVs, which were not reported by CMA (Supplemental Table S1).

Table 2: Results of SNP microarray in this study.

Sample	**SNP microarray findings**							**Identified by OGM using pipelines of CNV[1] and/or CSV[2]**
	Chromo-some	**Breakpoints**	**Breakpoint Start**	**Breakpoint Stop**	**Size (bp)**	**Abnormality Type (% mosaicism if applicable)^**	**Reported/ Pathogenic**	
1	chr 3	3p14.2	6,03,41,773	6,04,65,279	1,23,506	Loss (N/A)	No	Yes[1,2]
	chr 4	4q13.2	6,96,71,302	6,97,08,718	37,416	Loss (N/A)	No	Yes[2]
	chr 6	6p21.33	3,13,60,255	3,14,53,618	93,363	Loss (N/A)	No	Yes[2]
	chr 15	15q11.2	2,27,50,305	2,32,26,254	4,75,949	Gain (N/A)	No	Yes[1]
2	chr 2	2q12.3 to q14.3	10,74,93,000	12,78,95,000	2,04,02,000	Abnormal* (5-10%)	Yes	Yes[2]
	chr 2	2q22.1 to q23.3	14,22,10,000	15,35,00,000	1,12,90,000	Abnormal* (5-10%)	Yes	Yes[2]
	chr 2	2q35 to q37.1	21,82,30,000	23,13,90,000	1,31,60,000	Abnormal* (5-10%)	Yes	Yes[2]
	chr 6	6pter to p11.1	1,08,666	5,87,52,089	5,86,43,423	Gain (~15%)	Yes	No
	chr 6	6q11.1 to qter	6,18,91,118	17,09,19,470	10,90,28,352	CN-LOH (~15%)	Yes	No
	chr 11	11q14.3 to q22.1	8,92,85,550	10,06,24,538	1,13,38,988	Abnormal* (5-10%)	Yes	Yes[2]
	chr Y	Ypter to qter	whole	Chromosome	~ 58,000,000	Loss (~30%)	Yes	Yes[1]
3	chr 7	7p12.2	5,04,15,555	5,04,79,414	63,859	Loss (70-80%)	Yes	Yes[2]
	chr 9	9pter to p13.1	46,587	3,87,73,251	3,87,26,664	Loss (70-80%)	Yes	Yes[1]
	chr 9	9p21.3	2,10,73,945	2,22,93,804	12,19,859	Homozygous Loss (~95-100%)	Yes	Yes[2]
	chr 12	12p13.33 to p11.1	1,91,619	3,48,53,011	3,46,61,392	Loss (70-80%)	Yes	Yes[1]
	chr 12	12p13.2	1,18,04,717	1,20,55,043	2,50,326	Homozygous Loss (~95-100%)	Yes	Yes[1,2]
	chr 18	18p11.32	2,74,474	5,70,500	2,96,026	Loss (70-80%)	No	Yes[2]

4	chr 11	11p15.1	1,91,89,752	3,49,44,453	1,57,54,701	Loss (~50%)	Yes	Yes[1,2]
	chr 18	18p11.32	19,08,848	19,73,417	64,569	Loss (~40%)	No	Yes[2]
	chr X	Xpter to qter	whole	Chromosome	~ 155,000,000	Loss (~20%)	Yes	Yes[1]
	chr Y	Ypter to qter	whole	Chromosome	~ 58,000,000	"XY" Donor cells present	Yes	Yes[1]
5	chr 3	3p12.3 to p12.1	7,52,27,937	8,36,99,033	84,71,096	Loss (~40%)	Yes	Yes[2]
	chr 11	11pter to p15.4	1,98,510	63,55,016	61,56,506	Gain (~95-100%)	Yes	Yes[1]
	chr 11	11p15.4 to p13	63,62,948	3,17,93,051	2,54,30,103	CN-LOH (~95-100%)	Yes	No
	chr 14	14q23.1 to qter	6,10,72,875	10,72,87,663	4,62,14,788	Loss (~90%)	Yes	Yes[1]

Chr: chromosome; CN-LOH: copy-number neutral loss of heterozygosity; CNV: copy number variant pipeline; CSV: rare variant pipeline.
*"Abnormal" regions visible by SNP array, but present at a low frequency (5% -10%) and unable to be distinguished as gain, loss or CN-LOH. These abnormalities were identified visually due to a subtle change in the B-allele frequency plots; however, no visible difference in copy number change/LogR was identified or indicated by the software
^: Percent frequency is estimated based on B-allele frequency plots. Findings that show no clonal change (N/A) are estimated to be germline.

The 51 CNV calls included 25 deletions (49%) and 26 duplications (51%). For these 25 OGM deletion calls, 44% were detected by CMA and/or NGS and 56% were not detected (Figure 1A). OGM detected partial gene deletions that were not detected by CMA. For example, OGM revealed a 23 kb deletion including exon 1 and partial intron 1 of the *XBP1* gene (case 3, Figure 2A), which was confirmed by an NGS assay (Figure 2B-C). For these 26 OGM duplication calls, 27% were also detected by CMA and/or NGS and 73% were not detected by CMA/NGS (Figure 1B). The 20 SV calls included 8 interchromosomal translocations (40%), 7 insertions (35%), 4 intrachromosomal translocations (20%), and an inversion (5%). The majority of SV calls were not evaluated by targeted NGS/gene fusion assays/CMA because of no/limited coverage (Figure 1C).

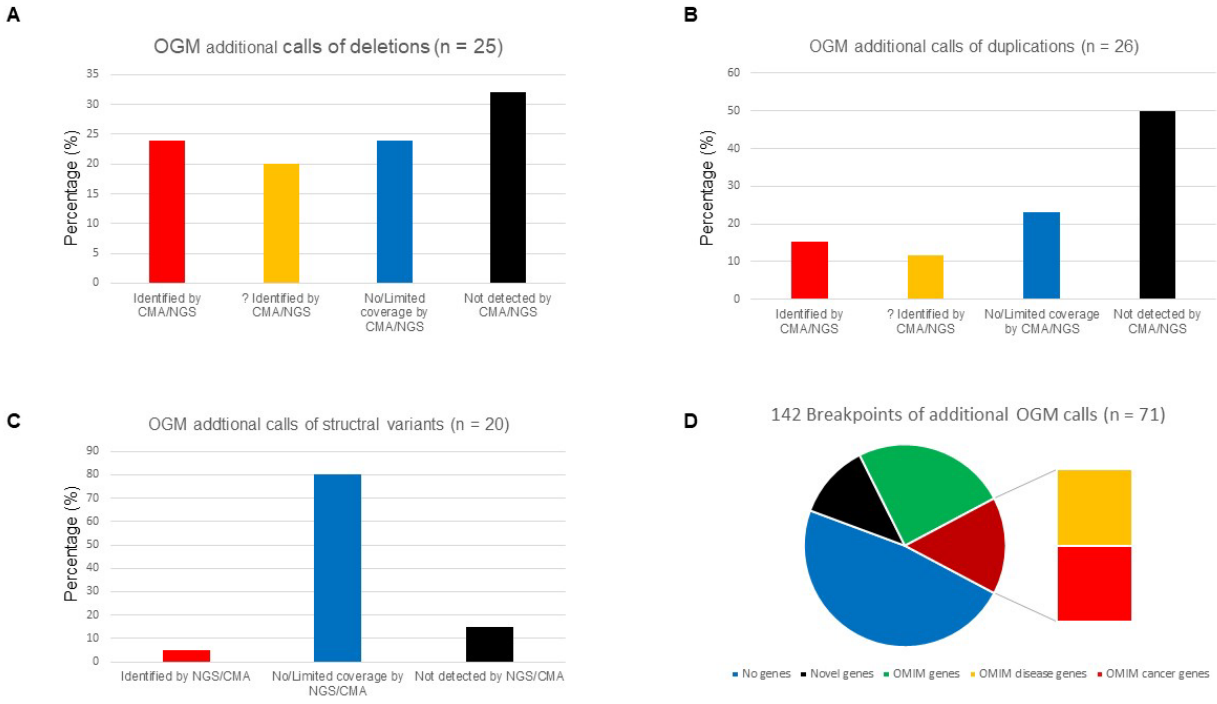

Figure 1: 71 Additional call by OGM. Yes (?): revealed by either NGS or CMA with slightly abnormal LogR and/or B-allele separation. OMIM: Online Mendelian Inheritance in Man.

Breakpoint analyses of additional calls revealed 74 (52%) breakpoints involved RefSeq genes (novel/non-cancer genes) and 68 (48%) breakpoints involved non-gene regions (Figure 1D). Among 74 breakpoints with RefSeq genes, ~ one-quarter involved novel/unknown genes, and ~ one-third involved OMIM disease genes (half of which had known genes involving gene fusions/ rearrangements in cancers) (Figure 1D). Repeat elements including LINEs, LTR elements, SINEs, DNA elements, and satellites were present in ~ 40% of breakpoints involved non-gene regions and in ~ 25% of breakpoints involved RefSeq genes. Overall, three of the additional calls (4.2%) contained cancer genes associated with patients' cancers and were reportable, and fifteen (21.1%, majority of SV calls with breakpoints involved novel/non-cancer genes and non-gene regions) were variants of unknown clinical significance (Supplemental Table S1).

Complex chromosome rearrangement/chromothripsis by OGM

OGM characterized two complex chromosome rearrangements in this study. Sample 5 had an abnormal chromosome 14 with additional genomic material added into the band of 14q23 by karyotype (Figure 3A), a gain of 11p15.4-pter, and loss of 14q23.1-qter by CMA (Figure 3B), and metaphase-FISH revealed 11p material on the abnormal chromosome 14 (Figure 3C). OGM detected an unbalanced 11;14 translocations with breakpoints of 11p15.4 (between *PRKCDBP* and *SMPD1* genes) and 14q23.1 (between *SIX6* and *SIX1* genes) in a Wilms tumor specimen (Figure

Citation: Stinnett V, Jiang L, Haley L, et al. (2021) Adoption of Optical Genome Mapping in Clinical Cancer Cytogenetic Laboratory: A Stepwise Approach. J Clin Anat Pathol, 6(2): 117. DOI: https://doi.org/10.47275/2332-4864-117

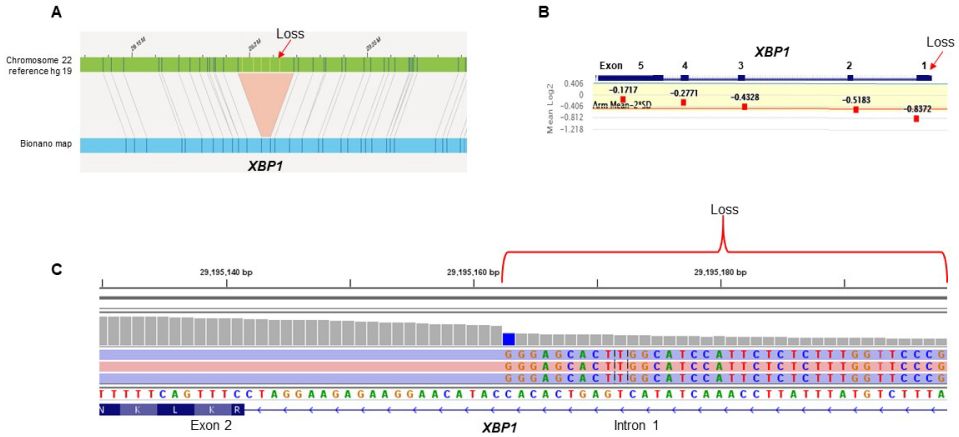

Figure 2: A partial deletion of *XBP1* in case 3. A. OGM revealed an exon 1 loss. B. Next-generation sequencing (NGS) confirmed this loss. C. NGS-reads show a deletion breakpoint at chr 22:29, 195, 163 (intron 1).

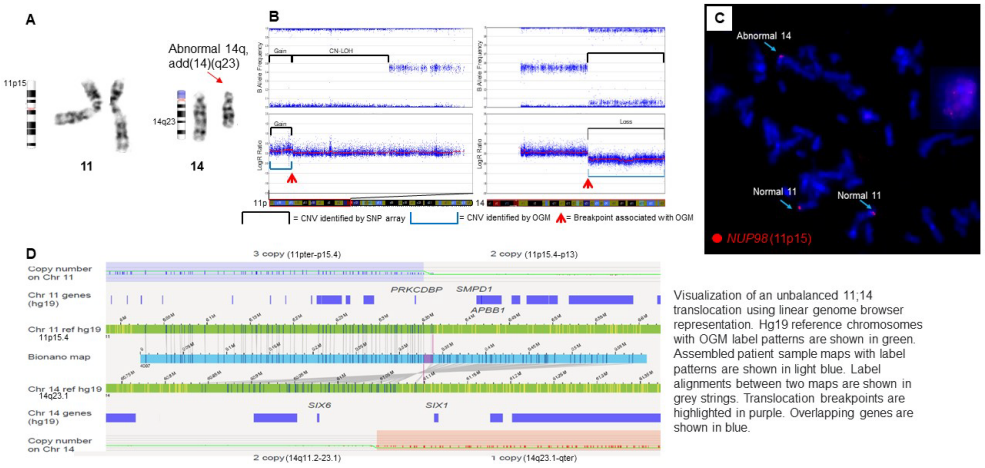

Figure 3: Abnormal chromosome 14q in case 5. A. Partial G-baned karyotype shows abnormal 14q. B. CMA shows loss of 14q and gain CN-LOH of 11p. C. Metaphase-FISH shows NUP98 (11p15) on abnormal chromosome 14q. D. OGM reveals unbalanced 11;14 translocation.

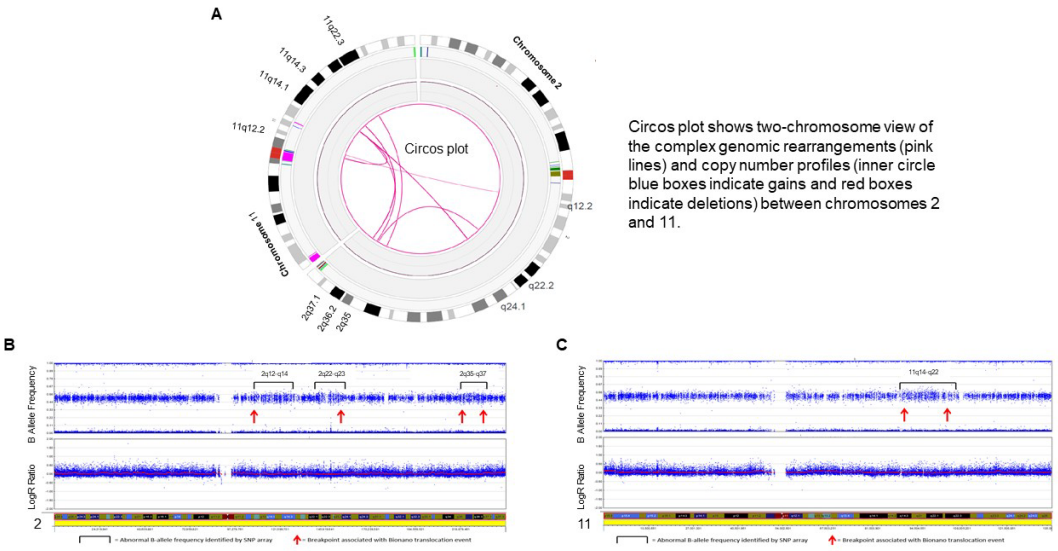

Figure 4: Chromothripsis-like event in case 2. A. Visualization of complex rearrangements by OGM. B-C. B-allele frequency of CMA shows subtle evidence of genomic rearrangements of chromosomes 2q and 11q.

3D). In sample 2, OGM revealed a chromothripsis-like event with multiple interchromosomal translocations between chromosomes 2q12.3-q37.1 and 11q12.2-q22.3 in a chronic lymphoblastic leukemia (CLL) specimen (Figure 4A), which were suggested by CMA (Figure 4B-C).

Discussion

This pilot study analyzed OGM calls blindly to assess efficacy as a clinical test in a clinical cancer cytogenetic laboratory. OGM detects genome-wide CNVs and SVs in cancer specimens at rates comparable to the combined standard of care routine cytogenetic techniques of karyotype/FISH/CMA assays. It revealed more CNVs and SVs calls compared to CMA. This preliminary study demonstrated a feasible approach to adopt OGM in a clinical diagnostic laboratory. For cancer cytogenetics technologists who routinely analyze CMA data, OGM calls can be easily analyzed and reported according to a procedure similar to that with which we analyze CMA calls. Therefore, OGM can be adopted smoothly into a clinical setting as a promising alternative to conventional cancer cytogenetics technologies.

Complex rearrangements and chromothripsis events are frequently challenging to determine by karyotype/FISH/CMA assays because of their complexity. OGM provided accuracy and insight into the precise structure of the SVs. It detected an unbalanced 11;14 translocations with breakpoints of 11p15.4 (between *PRKCDBP* and *SMPD1* genes) and 14q23.1 (between *SIX6* and *SIX1* genes) in a Wilms tumor specimen. The most common renal tumor of childhood, Wilms tumor is genetically heterogeneous [38]. Although the *SIX1* gene and 11p abnormalities have been reported in Wilms tumor [38,39], the unbalanced 11;14 translocations by OGM revealed a novel gene rearrangement/fusion, which may lead to developing blastemal type of Wilms tumor. OGM revealed a chromothripsis-like event involving chromosomes 2q12.3-2q37.1 and 11q14.3-q22.1 in a CLL patient. Chromothripsis has been indicated in the prevalence of genomic instability in high-risk, relapsed/refractory CLL [40]. Detection of chromothripsis in CLL might help in therapeutic decisions along the CLL clinical course. For CLL patients, the karyotype is limited by the low number of mitotic neoplastic cells [41], FISH is loci specific, and CMA cannot reveal balanced SVs. OGM can detect both CNVs and SVs across the genome, which makes it a more favored method for CLL patients in a clinical cancer cytogenetics laboratory.

OGM revealed additional CNV calls compared to CMA and can detect smaller CNVs even at an exon-level of cancer genes. For example, it detected a partial deletion of the X-box binding protein 1 (*XBP1*) gene in a B-cell acute lymphoblastic leukemia (ALL) specimen (case 3). Since pre-B ALL cells are uniquely vulnerable to endoplasmic reticulum stress, XBP1 as a downstream effector of the unfolded protein response pathway is identified as a novel therapeutic target to overcome drug resistance in pre-B ALL [42]. Homozygous deletion of *XBP1* has been reported to increase sensitivity to valosin-containing protein/p97 inhibitor, and the targeting of p97 is a novel promising therapeutic approach in B-cell ALL [43]. Therefore, an exon-level deletion of *XBP1* in B-cell ALL may have a potential treatment implication.

Besides well-known SVs in cancers, OGM also identified additional SV calls. Half of these SV breakpoints in this study involved novel genes, non-cancer genes, and upstream/downstream regions of genes. Although these unrecognized SVs may play significant roles in cancer development and formation, they are currently classified as variants of unknown clinical significance. However, with the accumulation of additional SV calls by OGM in various cancers, some of them may become recognized as recurrent abnormalities in specific types of cancers. Therefore, detection of genome-wide SVs by OGM may identify targetable genomic aberrations for novel breakthrough treatment options.

Conclusion

OGM is a reliable method for detecting both CNVs and SVs in cancer genomes using a stepwise approach and can be adopted smoothly into the clinical setting as a promising alternative to routine cytogenetic techniques of karyotype/FISH/CMA assays. It may reveal additional genome-wide CNV and SV calls compared to CMA, and these additional/unrecognized calls may play important roles in cancer development and formation. OGM can efficiently characterize complex chromosome rearrangements and/or chromothripsis events. Future work will involve comprehensively validating various abnormalities in cancers, improving the clinical analysis pipeline to determine clinical importance of additional calls, including potential candidate/novel cancer genes, and determining the optimal workflow for diagnostic purposes in a clinical cancer cytogenetics laboratory.

Acknowledgements

We would like to acknowledge Karl Hong, Alex Hastie, Andy Pang, and Alka Chaubey (Bionano Genomics Inc., San Diego, CA) for running OGM specimens on a Saphyr system and for using their variant analysis software (Bionano Access and Bionano Solve).

Funding

Departmental funding from Johns Hopkins University School of Medicine.

Declaration of competing interest

None declared.

References

1. Swerdlow SH, Campo E, Harris NL, Jaffe ES, Pileri SA, et al. (2017) WHO classification of tumours of haematopoietic and lymphoid tissues. (4th Edtn.). Int Agency Res Cancer 2.
2. Board WCoTE (2020) WHO classification of tumours, Soft tissue and bone tumours. (5th Edtn.) Int Agency Res Cancer 3.
3. Jiang LQ, Pallavajjala A, Huang JL, Haley L, Morsberger L, et al. (2021) Clinical utility of targeted next-generation sequencing assay to detect copy number variants associated with myelodysplastic syndrome in myeloid malignancies. J Mol Diagn 23: 467-483. https://doi.org/10.1016/j.jmoldx.2021.01.011
4. Barseghyan H, Tang W, Wang RT, Almalvez M, Segura E, et al. (2017) Next-generation mapping: a novel approach for detection of pathogenic structural variants with a potential utility in clinical diagnosis. Genome Med 9: 90. https://doi.org/10.1186/s13073-017-0479-0
5. Chaisson MJP, Sanders AD, Zhao X, Malhotra A, Porubsky D, et al. (2019) Multi-platform discovery of haplotype-resolved structural variation in human genomes. Nat Commun 10: 1784. https://doi.org/10.1038/s41467-018-08148-z

6. Levy-Sakin M, Pastor S, Mostovoy Y, Li L, Leung AKY, et al. (2019) Genome maps across 26 human populations reveal population-specific patterns of structural variation. Nat Commun 10: 1025. https://doi.org/10.1038/s41467-019-08992-7

7. Lin J, Qi R, Aston C, Jing J, Anantharaman TS, et al. (1999) Whole-genome shotgun optical mapping of Deinococcus radiodurans. Science 285: 1558-1562. https://doi.org/10.1126/science.285.5433.1558

8. Lim A, Dimalanta ET, Potamousis KD, Yen G, Apodoca J, et al. (2001) Shotgun optical maps of the whole Escherichia coli O157:H7 genome. Genome Res 11: 1584-1593. https://doi.org/10.1101/gr.172101

9. Zhou S, Wei F, Nguyen J, Bechner M, Potamousis K, et al. (2009) A single molecule scaffold for the maize genome. PLoS Genet 5: e1000711. https://doi.org/10.1371/journal.pgen.1000711

10. Jiao Y, Peluso P, Shi J, Liang T, Stitzer MC, et al. (2017) Improved maize reference genome with single-molecule technologies. Nature 546: 524-527. https://doi.org/10.1038/nature22971

11. Deschamps S, Zhang Y, Llaca V, Ye L, Sanyal A, et al. (2018) A chromosome-scale assembly of the sorghum genome using nanopore sequencing and optical mapping. Nat Commun 9: 4844. https://doi.org/10.1038/s41467-018-07271-1

12. Luo MC, Gu YQ, Puiu D, Wang H, Twardziok SO, et al. (2017) Genome sequence of the progenitor of the wheat D genome Aegilops tauschii. Nature 551: 498-502. https://doi.org/10.1038/nature24486

13. Paajanen P, Kettleborough G, Lopez-Girona E, Giolai M, Heavens D, et al. (2019) A critical comparison of technologies for a plant genome sequencing project. Gigascience 8: giy163. https://doi.org/10.1093/gigascience/giy163

14. Mak ACY, Lai YYY, Lam ET, Kwok TP, Leung AKY, et al. (2016) Genome-Wide structural variation detection by genome mapping on nanochannel arrays. Genetics 202: 351-362. https://doi.org/10.1534/genetics.115.183483

15. Hastie AR, Dong LL, Smith A, Finklestein J, Lam ET, et al. (2013) Rapid genome mapping in nanochannel arrays for highly complete and accurate de novo sequence assembly of the complex aegilops tauschii genome. Plos One 8: e55864. https://doi.org/10.1371/annotation/8629ed33-c566-4543-b657-eea1792f384c

16. Hastie A, Lam E, Dai H, Andrews W, Pang A, et al. (2014) Feasibility of population scale comprehensive identification and analysis of complex structural variations in cancer genome using nanochannel array. Blood 124: 476. https://doi.org/10.1182/blood.V124.21.476.476

17. Cao H, Hastie A, Pang A, Andrews W, Anantharaman T, et al. (2015) Mapping the dark matter of cancer genome - long repeats, complex structural variations with nanochannel technology. Cancer Research. 75: 4746. https://doi.org/10.1158/1538-7445.AM2015-4746

18. Cao H, Wu H, Luo R, Huang S, Sun Y, et al. (2015) De novo assembly of a haplotype-resolved human genome. Nat Biotechnol 33: 617-622. https://doi.org/10.1038/nbt.3200

19. Teague B, Waterman MS, Goldstein S, Potamousis K, Zhou S, et al. (2010) High-resolution human genome structure by single-molecule analysis. Proc Natl Acad Sci U S A 107: 10848-10853. https://doi.org/10.1073/pnas.0914638107

20. Sharim H, Grunwald A, Gabrieli T, Michaeli Y, Margalit S, et al. (2019) Long-read single-molecule maps of the functional methylome. Genome Res 29: 646-656. https://doi.org/10.1101/gr.240739.118

21. Wight DJ, Aimola G, Aswad A, Jill Lai CY, Bahamon C, et al. (2020) Unbiased optical mapping of telomere-integrated endogenous human herpesvirus 6. Proc Natl Acad Sci U S A 117: 31410-31416. https://doi.org/10.1073/pnas.2011872117

22. Demaerel W, Mostovoy Y, Yilmaz F, Vervoort L, Pastor S, et al. (2019) The 22q11 low copy repeats are characterized by unprecedented size and structural variability. Genome Res 29: 1389-1401. https://doi.org/10.1101/gr.248682.119

23. Zhang Q, Xu X, Ding L, Li H, Xu C, et al. (2019) Clinical application of single-molecule optical mapping to a multigeneration FSHD1 pedigree. Mol Genet Genomic Med 7: e565. https://doi.org/10.1002/mgg3.565

24. Dai Y, Li P, Wang Z, Liang F, Yang F, et al. (2020) Single-molecule optical mapping enables quantitative measurement of D4Z4 repeats in facioscapulohumeral muscular dystrophy (FSHD). J Med Genet 57: 109-120. http://dx.doi.org/10.1136/jmedgenet-2019-106078

25. Pastor S, Tran O, Jin A, Carrado D, Silva BA, et al. (2020) Optical mapping of the 22q11.2DS region reveals complex repeat structures and preferred locations for non-allelic homologous recombination (NAHR). Sci Rep 10: 12235. https://doi.org/10.1038/s41598-020-69134-4

26. Luebeck J, Coruh C, Dehkordi SR, Lange JT, Turner KM, et al. (2020) AmpliconReconstructor integrates NGS and optical mapping to resolve the complex structures of focal amplifications. Nat Commun. 11: 4374. https://doi.org/10.1038/s41467-020-18099-z

27. Antonacci F, Kidd JM, Marques-Bonet T, Teague B, Ventura M, et al. (2010) A large and complex structural polymorphism at 16p12.1 underlies microdeletion disease risk. Nat Genet 2: 745-750. https://doi.org/10.1038/ng.643

28. Maggiolini FAM, Cantsilieris S, D'Addabbo P, Manganelli M, Coe BP, et al. (2019) Genomic inversions and GOLGA core duplicons underlie disease instability at the 15q25 locus. PLoS Genet 15: e1008075. https://doi.org/10.1371/journal.pgen.1008075

29. Zook JM, Hansen NF, Olson ND, Chapman L, Mullikin JC, et al. (2020) A robust benchmark for detection of germline large deletions and insertions. Nat Biotechnol 38: 1347-1355. https://doi.org/10.1038/s41587-020-0538-8

30. Ray M, Goldstein S, Zhou S, Potamousis K, Sarkar D, et al. (2013) Discovery of structural alterations in solid tumor oligodendroglioma by single molecule analysis. BMC Genomics 14: 505. https://doi.org/10.1186/1471-2164-14-505

31. Gupta A, Place M, Goldstein S, Sarkar D, Zhou S, et al. (2015) Single-molecule analysis reveals widespread structural variation in multiple myeloma. Proc Natl Acad Sci U S A. 112: 7689-7694. https://doi.org/10.1073/pnas.1418577112

32. Goldrich DY, LaBarge B, Chartrand S, Zhang L, Sadowski HB, et al. (2021) Identification of somatic structural variants in solid tumors by optical genome mapping. J Pers Med 11: 142. https://doi.org/10.3390/jpm11020142

33. Dixon JR, Xu J, Dileep V, Zhan Y, Song F, et al. (2018) Integrative detection and analysis of structural variation in cancer genomes. Nat Genet 50: 1388-1398. https://doi.org/10.1038/s41588-018-0195-8

34. Chan EKF, Cameron DL, Petersen DC, Lyons RJ, Baldi BF, et al. (2018) Optical mapping reveals a higher level of genomic architecture of chained fusions in cancer. Genome Res 28: 726-738. https://doi.org/10.1101/gr.227975.117

35. Du C, Mark D, Wappenschmidt B, Bockmann B, Pabst B, et al. (2018) A tandem duplication of BRCA1 exons 1-19 through DHX8 exon 2 in four families with hereditary breast and ovarian cancer syndrome. Breast Cancer Res Treat 172: 561-569. https://doi.org/10.1007/s10549-018-4957-x

Citation: Stinnett V, Jiang L, Haley L, et al. (2021) Adoption of Optical Genome Mapping in Clinical Cancer Cytogenetic Laboratory: A Stepwise Approach. J Clin Anat Pathol, 6(2): 117. DOI: https://doi.org/10.47275/2332-4864-117

36. Jaratlerdsiri W, Chan EKF, Petersen DC, Yang C, Croucher PI, et al. (2017) Next generation mapping reveals novel large genomic rearrangements in prostate cancer. Oncotarget 84: 23588-23602. https://doi.org/10.18632/oncotarget.15802

37. Neveling K, Mantere T, Kater-Baats E, van Beek R, Oorsprong M, et al. 2020. Next generation cytogenetics: genome-imaging enables comprehensive structural variant detection for 100 constitutional chromosomal aberrations in 85 samples. bioRxiv Genet. https://doi.org/10.1101/2020.07.15.205245

38. Treger TD, Chowdhury T, Pritchard-Jones K, Behjati S (2019) The genetic changes of Wilms tumour. Nat Rev Nephrol 15: 240-251. https://doi.org/10.1038/s41581-019-0112-0

39. Sehic D, Karlsson J, Sandstedt B, Gisselsson D (2012) SIX1 protein expression selectively identifies blastemal elements in Wilms tumor. Pediatr Blood Cancer 59: 62-68. https://doi.org/10.1002/pbc.24025

40. Steinbrecher D, Jebaraj BMC, Schneider C, Edelmann J, Cymbalista F, et al. (2018) Telomere length in poor-risk chronic lymphocytic leukemia: associations with disease characteristics and outcome. Leuk Lymphoma 59: 1614-1623. https://doi.org/10.1080/10428194.2017.1390236

41. Goorha S, Glenn MJ, Drozd-Borysiuk E, Chen Z (2004) A set of commercially available fluorescent in-situ hybridization probes efficiently detects cytogenetic abnormalities in patients with chronic lymphocytic leukemia. Genet Med 6: 48-53. https://doi.org/10.1097/01.GIM.0000105741.57923.08

42. Kharabi Masouleh B, Geng H, Hurtz C, Chan LN, Logan AC, et al. (2014) Mechanistic rationale for targeting the unfolded protein response in pre-B acute lymphoblastic leukemia. Proc Natl Acad Sci U S A 111: E2219-2228. https://doi.org/10.1073/pnas.1400958111

43. Gugliotta G, Sudo M, Cao Q, Lin DC, Sun H, et al. (2017) Valosin-containing protein/p97 as a novel therapeutic target in acute lymphoblastic leukemia. Neoplasia 19: 750-761. https://doi.org/10.1016/j.neo.2017.08.001